J|A|C|S
ARTICLES
Published on Web 11/22/2003

HYSCORE Spectroscopy in the Cytochrome b_{559} of the Photosystem II Reaction Center

Inés García-Rubio,[†,‡] Jesús I. Martínez,[†] Rafael Picorel,[§] Inmaculada Yruela,[§] and Pablo J. Alonso*[,†]

Instituto de Ciencia de Materiales de Aragón, Consejo Superior de Investigaciones Científicas, Universidad de Zaragoza, Plaza S. Francisco s/n, E-50009 Zaragoza, Spain, and Estación Experimental de Aula Dei, Consejo Superior de Investigaciones Científicas, Apartado 202, E-50080 Zaragoza, Spain

Received March 28, 2003; E-mail: alonso@unizar.es

Abstract: A HYSCORE investigation of the heme center in the cytochrome b_{559} is presented. To assign the observed signals to specific nuclei, bis-imidazol coordinated heme compounds that model the iron environment in cytochrome b_{559} are also studied. In the model compounds selective isotopic substitution of nitrogen atoms has been performed. The HYSCORE spectra allow us to obtain the hyperfine and quadrupolar coupling tensors of heme and imidazol bonding nitrogen atoms. The results can be interpreted in terms of the structure and the electronic distribution of the active center. The hyperfine tensors indicate that the unpaired electron is confined in a nonbonding iron orbital with a negligible nitrogen p orbital contribution. Quadrupolar coupling tensors suggest that the orientation of the semioccupied orbital is driven by the orientation of the two parallel imidazol rings of the axial histidine side chains. The results are discussed in terms of the structure−function relationship of cytochromes.

I. Introduction

Cytochromes are electron-transfer heme proteins that are involved in many biochemical processes. They exhibit a large variety of redox potentials. This characteristic allows them to act as electron carriers in many different metabolic reactions and other processes that take place in living organisms. The relationship between the electronic structure of the heme group (either the final acceptor or the first donor in the redox reactions of cytochromes) and the reaction mechanisms of cytochromes is not well understood in most cases.

Because the ferric state of cytochromes is paramagnetic, electron paramagnetic resonance (EPR) techniques have been used to characterize these kinds of proteins. Continuous wave EPR (CW-EPR) spectroscopy gives useful information about the unpaired electronic distribution in the heme center.[1] Nevertheless, no information about the hyperfine and quadrupolar interaction with the neighboring nuclei can be obtained by this conventional technique because of its lack of resolution. From these interactions we can learn more about the structure and electronic properties of the heminic center. Because of this, electron nuclear double resonance (ENDOR) and, more scarcely, electron spin−echo envelope modulation (ESEEM) techniques have been applied to study different heminic systems, both in heme proteins and heme model systems.[2−8]

When using these techniques, it has to be taken into account that in heme proteins the Fe^{3+} paramagnetic entity is surrounded by a lot of magnetic nuclei (five or six nitrogen and several protons) and all of them are able to weakly interact with the unpaired electron. Performing selective isotopic substitution would lead to a direct assignment of the signals to particular nuclei, but in practice this is not always achievable when working with biological materials. In this case the use of model systems can be useful. Moreover, protein samples are orientationally disordered in most cases. Thus, the corresponding signals in ENDOR as well as in one-dimensional (1D) ESEEM spectra strongly overlap and are consequently very difficult to disentangle.

On the other hand, the two-dimensional (2D) ESEEM HYSCORE spectroscopy introduced some years ago[9] has proved to be useful in studying weak hyperfine interactions with many nuclei in orientationally disordered systems.[10−12] Nevertheless,

* Corresponding author.
[†] Instituto de Ciencia de Materiales de Aragón, CSIC, Universidad de Zaragoza.
[‡] Current address: Laboratory of Physical Chemistry, ETH Hönggerberg, CH-8093 Zürich, Switzerland.
[§] Estación Experimental de Aula Dei, CSIC.

(1) Taylor, C. P. S. *Biochim. Biophys. Acta* **1977**, *491*, 137−149.
(2) Scholes, C. P.; Van Camp, H. L. *Biophys. Biochim. Acta* **1976**, *434*, 290−296.
(3) Scholes, C. P.; Falkovski, K. M.; Che, S.; Bank, J. *J. Am. Chem. Soc.* **1986**, *106*, 1660−1671.
(4) Fahnenschmidt, M.; Rau, H. K.; Bittl, R.; Haehnel, W.; Lubitz, W. *Chem. Eur. J.* **1999**, *5*, 2327−2334.
(5) Fahnenschmidt, M.; Bittl, R.; Rau, H. K.; Haehnel, W.; Lubitz, W. *Chem. Phys. Lett.* **2000**, *323*, 329−339.
(6) Magliozzo, R.; Peisach, J. *Biochemistry* **1992**, *31*, 189−199.
(7) Magliozzo, R.; Peisach, J. *Biochemistry* **1993**, *32*, 8446−8456.
(8) Peisach, J.; Mims, W. B.; Davis, J. L. *J. Biol. Chem.* **1979**, *254*, 12379−12389.
(9) Höfer, P.; Grupp, A.; Nebenführ, H.; Mehring, M. *Chem. Phys. Lett.* **1986**, *132*, 279.

10.1021/ja035364g CCC: $25.00

the potential of the HYSCORE technique has not yet been fully exploited to study heminic systems.[13,14]

In this work, we examine the ferric state of cytochrome (Cyt) b_{559} from spinach by means of the HYSCORE technique. Cyt b_{559} is a heme protein constituent of the photosystem II (PSII) reaction center (RC), which is tightly bound to the D1 and D2 polypeptides of the PSII RC. We have studied Cyt b_{559} in D1−D2−Cyt b_{559} reaction center complexes, the minimum PSII complexes with which efficient light-induced primary charge separation can be performed. This heme protein consists of two small polypeptides, the α (9 kDa) and β (4.5 kDa) subunits with a transmembrane α-helical domain and heterodimeric structure.[15−17] Two histidine residues (α-His22 and β-His17), placed axially with respect to the porphyrin ring, within the hydrophobic domain of each polypeptide act as ligands of the heme iron.

Over the past few years a great effort has been made to understand the function of Cyt b_{559} in the PSII RC and the relationship between the possible roles proposed and its structure. Despite the numerous studies performed,[18−20] the exact function of Cyt b_{559} is still unclear but the following possibilities have been proposed: (i) Cyt b_{559} is involved in the electron-transfer reactions on the oxidizing side of PSII, (ii) it participates in the assembly of the water-splitting system, and (iii) it plays a role in the protection of PSII against photoinhibition.[15] It is well-known that Cyt b_{559} can exist in a number of different redox forms. In chloroplasts, thylakoids, and oxygen-evolving PSII membrane fragments, where PSII complexes are surrounded by their natural membrane environments, Cyt b_{559} exhibits several midpoint redox potential (E'_m) Cyt b_{559} forms: +400 mV (the high-potential, HP, form), +200 to +150 mV (the intermediate potential, IP, form), and +70 to +60 mV (the low-potential, LP, form).[15,21−23]

Cyt b_{559} was characterized by EPR spectroscopy a few years ago.[15] Its CW-EPR spectra are typical of a low-spin heme iron and can be described with an effective spin $S = 1/2$ and an orthorhombic g-tensor with the following principal values: $g_X \approx 1.5$, $g_Y \approx 2.3$, and $g_Z \approx 3.0$. Slight modifications of the g_Z-value depending on the preparation and purification of the samples have been described.[15] These minor differences in the CW-EPR spectra were related with changes between different redox forms of Cyt b_{559}.[15] Thompson[24] suggested the existence of small changes in the iron neighborhood as the reason for the g_Z-modification. Recent studies[25] point out that some small changes in the Cyt b_{559} CW-EPR spectrum are related to the conditions of the detergent used to stabilize the PSII RC samples.

With those antecedents we have undertaken the present HYSCORE study of Cyt b_{559}. This technique allows one to obtain detailed information about the interactions among iron and the nearby nitrogen atoms. These interactions provide information concerning the structure, the electronic distribution, and the factors that determine these properties. This can clarify the connection of structure and electronic distribution to other properties, as well as their relevance on the Cyt b_{559} function. Furthermore, from a general point of view, with this study we intend to determine the ability of this technique to study low-spin heme proteins. Efforts made in this direction are worthy because, as other authors[26] have pointed out, "the knowledge of the electronic properties and the understanding of their relationship with other significant properties are functionally relevant".

In our case, it is not possible to work with selectively labeled Cyt b_{559}. Thus, to accomplish our goal, we take advantage of working with model compounds that mimic the heme center of the protein and consequently have similar CW-EPR and HYSCORE spectra. By selective isotopic substitution of iron bonding nitrogen atoms in these simpler systems, a direct assignment of the HYSCORE correlation peaks was done. Because of the similarity of the spectra, this assignment can be extended to the Cyt b_{559}. The hyperfine and quadrupolar coupling tensors corresponding to each nucleus can be obtained from these spectra. The coupling tensors are interpreted in terms of the structure and electronic distribution of this protein.

II. Materials and Methods

Cytochrome b_{559} Preparation. Cyt b_{559} was studied in standard D1−D2−Cyt b_{559} reaction center complex preparations isolated from highly purified oxygen-evolving PSII membranes from market spinach[27] according to the procedure described previously.[28] This method makes use of a Q-Sepharose fast-flow column (Amersham Biosciences). PSII membranes previously solubilized with 4% (w/v) Triton X-100 were loaded in the column and washed with 0.15% (w/v) Triton X-100. This procedure was continued until the absorbance at 417 nm was higher than that at 435 nm. The detergent was subsequently exchanged by *n*-dodecyl-β-D-maltoside (β-DM) at different concentrations ranging from 0 to 0.2% (w/v) in buffer 50 mM 2-(*N*-morpholino)ethanesulfonic acid (Mes-NaOH), pH 6.5. Since the HYSCORE spectra showed no dependence on β-DM concentration, a typical value of 0.1% (w/v) was used. Detergent replacement was carried out until Triton X-100 absorbance at 280 nm was lower than 0.01. Then, D1−D2−Cyt b_{559} reaction center complexes were collected at 1 mL/min and subsequently concentrated by centrifugation at 5000*g* in Centripep-30 and Centricon-30 (Amicon) tubes to reach a final concentration of 0.5−1.0 mM. Once concentrated samples were transferred to quartz tubes, they were stored at 77 K until use. Potentiometric redox titrations yielded midpoint

(10) Shane, J. J.; Höfer, P.; Reijerse, E. J.; de Boer, E. *J. Magn. Reson.* **1992**, *99*, 596−602.
(11) Martínez, J. I.; Alonso, P. J.; Gómez-Moreno, C.; Medina, M. *Biochemistry* **1997**, *36*, 15526−15537.
(12) Schweiger, A.; Jeschke, G. *Principles of Pulse Electron Paramagnetic Resonance*; Oxford University Press: Oxford, U.K., 2001.
(13) Gilbert, D. C.; Dikanov, S. A.; Doetschman, D. C.; Smeija, J. A. *Chem. Phys. Lett.* **1999**, *315*, 43−48.
(14) Tyryshkin, A. M.; Dikanov, S. A.; Reijerse, E. J.; Burgard, C.; Hüttermann, J. *J. Am. Chem. Soc.* **1999**, *121*, 3396−3406.
(15) Stewart, D. M.; Brudvig, G. W. *Biochim. Biophys. Acta* **1998**, *1367*, 63−87.
(16) Zouni, A.; Witt, H.-T.; Kern, J.; Fromme, P.; Krausse, N.; Saenger, W.; Orth, P. *Nature* **2001**, *409*, 739−743.
(17) Kamiya, N.; Shen, J.-R. *Proc. Natl. Acad. Sci. U.S.A.* **2003**, *100*, 98−103.
(18) Cramer, W. A.; Whitmarsh, J. *Annu. Rev. Plant Physiol.* **1997**, *28*, 133−172.
(19) Shuvalov, V. A. *J. Bioenerg. Biomembr.* **1994**, *26*, 619−626.
(20) Whitmarsh, J.; Pakrasi, H. B. *Form and Function of Cytochrome b559*. In *Oxygenic Photosynthesis: The Light Reactions*; Ort, D, R., Yocum, C. F., Eds.; Kluwer: Dordrecht, The Netherlands, 1996; pp 249−264.
(21) Kaminskaya, O.; Kurreck, J.; Irrgang, K.-D.; Renger, G.; Shuvalov, V. A. *Biochemistry* **1999**, *38*, 16223−16235.
(22) Mizusawa, N.; Yamashita, T.; Miyao, M. *Biochim. Biophys. Acta* **1999**, *1410*, 273−286.
(23) Roncel, M.; Ortega, J. M.; Losada, M. *Eur. J. Biochem.* **2001**, *268*, 4961−4968.
(24) Thompson, L. K.; Miller, A.; Buser, C. A.; De Paula, J. C.; Brudvig, G. W. *Biochemistry* **1989**, *28*, 8048−8056.
(25) Yruela, I.; García-Rubio, I.; Roncel, M.; Martínez, J. I.; Ramiro, M. V.; Ortega, J. M.; Alonso, P. J.; Picorel, R. *Photochem. Photobiol. Sci.* **2003**, *2*, 437−442.
(26) Lowe, D. J. *ENDOR and EPR of Metalloproteins*; Springer: New York, 1995.
(27) Berthold, D. A.; Babcock, G. T.; Yocum, C. F. *FEBS Lett.* **1981**, *134*, 231−234.
(28) Yruela, I.; van Kan, P. J. M.; Müller, M. G.; Holzwarth, A. R. *FEBS Lett.* **1994**, *339*, 25−30.

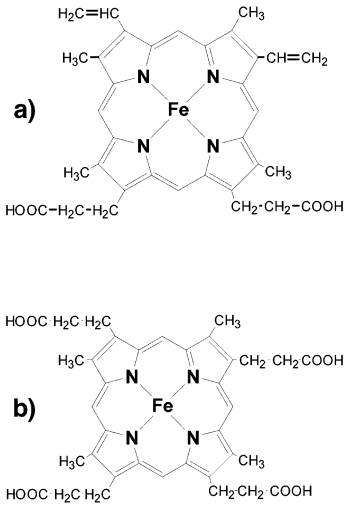

Figure 1. (a) Iron(III)−protoporphyrin IX (PPIX) and heme *b*. (b) Iron(III)−[^{15}N]coproporphyrin III ([^{15}N]CPIII).

reduction potentials in the range of 123−150 (±15) mV for all the samples, irrespective of the detergent content.[25]

Model Compound. For preparing model compounds the following reagents were used: iron(III)−protoporphyrin IX (PPIX) (see Figure 1a) from Sigma (purity > 80%); iron(III)−[^{15}N]coproporphyrin III ([^{15}N]CPIII; see Figure 1b) from Porphyrin Products Co. (^{15}N enrichment higher than 99%); imidazol (Im) from Fluka (purity > 99.5%); [^{15}N]imidazol ([^{15}N]Im) from Aldrich Chemical Co. (^{15}N enrichment higher than 99%). The iron−porphyrin complexes and imidazol were dissolved in dimethyl sulfoxide, DMSO (1:10), and then $CHCl_3$ was added to duplicate the solution volume. It is known[3] that this reagent proportion yields a bis-imidazol heme coordination. The final concentration of the Fe(III)−P(Im)$_2$ was about 10 mM. Homogenized solutions were transferred to quartz tubes, frozen, and stored in liquid nitrogen for later measurement.

EPR/ESEEM Measurements. An ESP380E spectrometer from Bruker working in X-band was used for the ESEEM measurements. The 1D- and 2D-ESEEM spectra were taken at temperatures in the 6−10 K range. An Oxford CF935 continuous-flow cryostat was used. Samples, kept in quartz tubes (707-SQ) from Wilmad Labglass at liquid nitrogen temperature, were transferred into the resonant cavity without significant warming up.

Microwave pulse sequences were ($\pi/2 - \tau - \pi/2 - t - \pi/2 - \tau$) and ($\pi/2 - \tau - \pi/2 - t - \pi - t - \pi/2 - \tau$) for the three pulses (3*p*) and four pulses (4*p*) 1D-ESEEM experiments, respectively; the time t was varied with a sampling interval of 16 ns (Nyquist frequency of 31.25 MHz), and 1024 experimental points were collected. For the 2D-HYSCORE experiments, the four-pulses ($\pi/2 - \tau - \pi/2 - t_1 - \pi - t_2 - \pi/2 - \tau$) sequence was used and t_1 and t_2 were varied independently with a sampling time of 16 or 48 ns (Nyquist frequency of 31.25 and 10.41 MHz, respectively). In this case two-dimensional arrays were obtained. The width of the $\pi/2$ pulse was 16 ns for the three-pulse ESEEM experiments and 24 ns for the four-pulse experiments where the inversion pulse was 16 ns long. In HYSCORE experiments typical values of τ were 96 and 208 ns whereas 1D-ESEEM experiments were performed for τ values of 96, 144, and 208 ns. Appropriate phase cycling was applied to minimize the contribution of unwanted echoes.

Data Handling/Processing. The 1D and 2D frequency domain spectra were obtained with the WIN-EPR program from Bruker. Background contributions, simulated by a polynomial up to sixth degree, were subtracted to the raw time-domain signals prior to any treatment. Then, after windowing with a Hamming digital filter, a fast Fourier transform algorithm was applied to get the frequency-domain signals. The application of the digital filter improves the signal-to-noise ratio without any significant reduction of resolution. The spectra correspond to the modulus of the Fourier transform. The simulated spectra were obtained using a computer program written in our laboratory[29] and adapted for orientation selection experiments, which provides both the position and amplitude of the correlation signals.

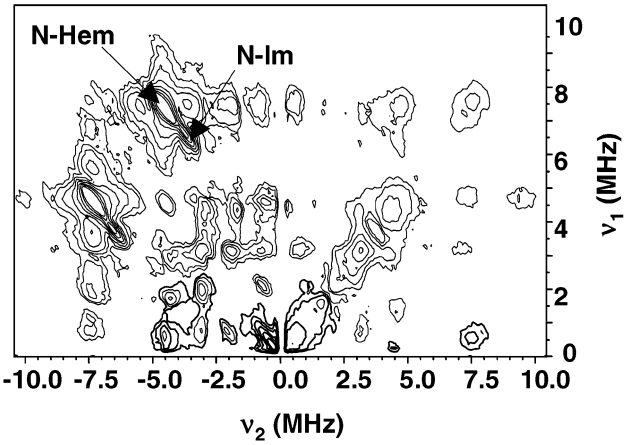

Figure 2. g_Z-HYSCORE spectrum of a ^{14}N naturally abundant model compound sample (for details see Materials and Methods). The static magnetic field was set at 234 mT, and the time separation between the two first pulses was $\tau = 96$ ns. The **dq**−**dq** correlations due to N-Im and N-Hem are indicated. Features at higher frequencies are shown in the Supporting Information.

III. Experimental Results

Model Compound. The CW-EPR spectrum of a frozen solution of a model compound shows three clearly resolved features associated with the principal values of an orthorhombic g-tensor of an effective spin $S = 1/2$ entity. This description is very common for Fe^{3+} bound to a porphyrin ring in a low-spin configuration.[30] The actual g-tensor principal values are $g_X = 1.52 \pm 0.02$, $g_Y = 2.25 \pm 0.01$, and $g_Z = 2.98 \pm 0.02$, which are typical of a bis-imidazol coordinated heme center with parallel axial ligands.[30−32] Selectively ^{15}N labeled compounds show the same CW-EPR spectrum. The strong anisotropy of this spectrum allows us to make orientation selection ESEEM experiments.[12] In particular, we have done these experiments for magnetic fields corresponding to the principal values of the g-tensor. Hereafter, and for the shake of brevity, the corresponding nuclear spectra in the frequency domain will be called g_X-, g_Y-, and g_Z-spectra. Since g_X and g_Z are extreme values of the effective g-factor, the g_X- and g_Z-spectra are single-crystal-like spectra. On the other hand, all the molecules for which the effective g-factor nearly coincides with g_Y contribute to the g_Y-spectra, and consequently these are multiorientation spectra.

One of the g_Z-HYSCORE spectra measured in a naturally abundant isotopic content model compound is shown in Figure 2. The most intense features are two pairs of correlation peaks in the second quadrant associated with ^{14}N. Hereafter, we adopt the convention of putting a minus sign in one of the correlation frequencies to mean that the correlation appears in the second quadrant. By comparison with the signals observed in ^{15}N-labeled samples either in the imidazol ring or in the porphyrin

(29) Alonso, P. J.; Antorrena, G.; Martínez, J. I.; Novoa, J. J.; Palacio, F.; Rawson, J. M.; Smith, J. N. B. *Appl. Magn. Reson.* **2001**, *20*, 231.
(30) Walker, F. A. *Coord. Chem. Rev.* **1999**, *185*−*186*, 471−534.
(31) Walker, F. A.; Huynh, B. H.; Scheid, W. R.; Osvath, R. S. *J. Am. Chem. Soc.* **1986**, *108*, 5288−5297.
(32) Astashkin, A. V.; Raitsimring, A. M.; Walker, F. A. *J. Am. Chem. Soc.* **2001**, *123*, 1905−1913.

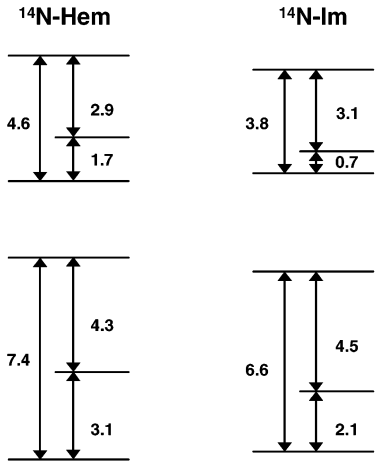

Figure 3. Scheme of the splitting of the nuclear sublevels for [^{14}N]Hem and [^{14}N]Im nuclei with an orientation of the magnetic field along the *Z*-axis. The frequencies of the nuclear transitions are given in MHz.

Table 1. Correlations Observed in the g_Z-HYSCORE Spectra of the Model Compounds (Solid Squares, Signals Assigned to ^{15}N or to ^{14}N **dq**−**dq** Correlations; Open Squares, Other ^{14}N Correlations; Precision, ±0.2 MHz)

peak freq (MHz)	^{14}N both	[^{15}N]Hem	[^{15}N]Im	^{15}N both
14.8, 9.2	□		□	
14.0, 8.4	□			
7.4, 4.6	■		■	
7.4, 2.9	□		□	
7.4, 1.7			□	
6.6, 3.8	■	■		
5.0, 3.0		■		■
4.6, 3.1	□		□	
4.5, 3.1	□	□		
4.5, 2.5			■	■
4.5, 0.7	□	□		
4.3, 1.7	□		□	
3.8, 2.1		□		
3.1, 2.9	□		□	
3.1, 2.1	□	□		
3.1, 1.7			□	
3.1, 0.7	□	□		
2.1, 0.7	□	□		

(see Supporting Information) the signal in (7.4 MHz, −4.6 MHz) is assigned to [^{14}N]porphyrin and the one in (6.6 MHz, −3.8 MHz) to [^{14}N]imidazol. It is worth noting that the frequency difference is 2.8 MHz in both cases, namely, four times the Larmor frequency (0.7 MHz). This strongly suggests that those signals are associated with the correlation between $\Delta M_I = \pm 2$ transitions in both electron spin manifolds (hereafter named double quantum, **dq**, transitions).

Other less intense peaks appear at lower frequencies. These are associated with correlations between $\Delta M_I = \pm 1$ transitions (called single quantum, **sq**, transitions) in both spin manifolds or to **sq**−**dq** correlations. The frequencies of all the observed correlation peaks in g_Z-HYSCORE spectra for the different measured samples (regardless of the quadrant) are collected in Table 1. A detailed comparison of these spectra allowed us to assign the spectral features either to the porphyrin (N-Hem) or to the imidazol (N-Im) nitrogen nuclei. All the correlation peaks can be explained with two sets of nitrogen nuclear transitions (see Figure 3). This suggests the equivalence of the two imidazol axial ligands as well as the equivalence of the four porphyrin nitrogen nuclei for this orientation of the magnetic field. It has been shown[33,34] that this orientation corresponds to the normal of the heme plane (which is the g_Z principal direction) for bis-imidazol-coordinated heme centers.

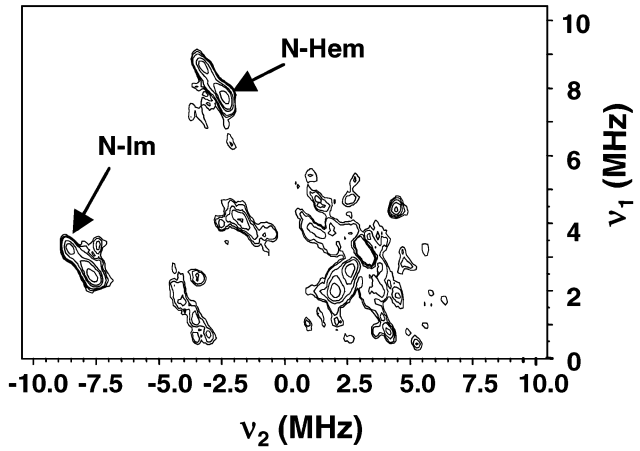

Figure 4. g_X-HYSCORE spectrum of a ^{14}N naturally abundant model compound sample (for details see Materials and Methods). The static magnetic field was set at 455 mT, and the time separation between the two first pulses was $\tau = 96$ ns. The **dq**−**dq** correlations due to N-Im and N-Hem are indicated.

A correlation around (10 MHz, 10 MHz) is also observed in the first quadrant (see Supporting Information), which is associated with some interacting protons.

The g_X-HYSCORE spectra are also crystal-like but in this case the orientation of the principal *X*-axis (that has to be in the heme plane) is a priori unknown. g_X-spectra also display intense **dq**−**dq** correlation peaks and several features associated with **sq** transitions at lower frequencies (see Figure 4). It is interesting to note that the latter correlations are not peaks as we found for g_Z-spectra but rather display an extended shape as little ridges.

The detected correlation features (regardless of the quadrant) for all samples are summarized in Table 2, and they can be assigned either to the porphyrin (N-Hem) or to the imidazol (N-Im) nitrogen nuclei. g_X-HYSCORE spectra of selectively labeled samples are collected in the Supporting Information. As in the former case only one set of correlation peaks is needed to account for the nuclear frequencies associated with imidazol nitrogen nuclei, indicating that both nitrogen atoms are also equivalent for this orientation of the magnetic field. The signal at (8.6 MHz, −3.3 MHz) is associated with the **dq**−**dq** correlation of [^{14}N]Im; the peak at (17.2 MHz, −3.3 MHz) is associated with a **2dq**−**dq** correlation, and its observation clearly indicates that we are dealing with two equivalent imidazol nitrogen atoms.

Although there is only one strong signal associated with a **dq**−**dq** [^{14}N]Hem correlation (7.7 MHz, −2.5 MHz), two sets of nuclear frequencies have to be considered to account for the [^{14}N]Hem correlation peaks involving **sq** transition frequencies. The existence of these two sets indicates that there are two nonequivalent pairs of porphyrin nitrogen atoms. We will see later that the shape of the **dq**−**dq** transitions observed in the g_Y-spectrum supports this hypothesis.

Taking into account the nuclear frequencies obtained from the spectra (Table 2), we have worked out the two sets of [^{14}N]-

(33) Hori, H. *Biochim. Biophys. Acta* **1971**, *251*, 227−235.
(34) Quinn, R.; Valentine, J. S.; Byrn, M. P.; Strouse, C. E. *J. Am. Chem. Soc.* **1987**, *109*, 3301−3308.

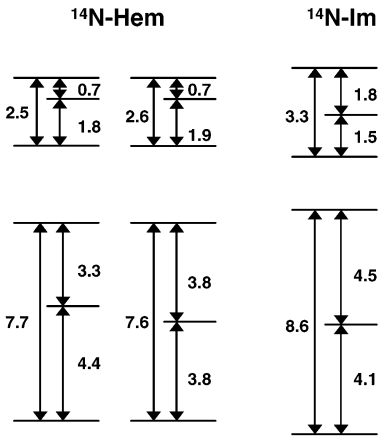

Figure 5. As in Figure 3 but with orientation of the magnetic field along the *X*-axis. The two nonequivalent sets of N-Hem nuclei (see text) are shown. The frequencies of the nuclear transitions are given in megahertz.

Table 2. Correlations Observed in the g_X-HYSCORE Spectra of the Model Compounds (Solid Squares, Signals Assigned to ^{15}N or to ^{14}N **dq**−**dq** Correlations; Open Squares, Other ^{14}N Correlations; Precision, ±0.2 MHz)

peak freq (MHz)	^{14}N both	[^{15}N]He m	[^{15}N]Im	^{15}N both
17.2, 3.3		□		
8.6, 3.3	■	■		
8.6, 1.5		□		
7.7, 2.5	■		■	
7.7, 1.8			□	
5.8, 2.0			■	■
5.4, 3.2		□		
5.4, 2.0		□		
5.4, 1.5		■		■
4.4, 2.5	□		□	
4.4, 1.8	□		□	
4.4, 1.5		□		
4.4, 0.7	□		□	
3.8, 2.6	□		□	
3.8, 1.9	□		□	
3.8, 0.7	□		□	
3.3, 2.5	□		□	
3.3, 1.8	□		□	
3.3, 1.5		□		
2.5, 0.5	□		□	

Hem nuclear frequencies that are shown in Figure 5. All the correlation peaks, except the one appearing at (2.5 MHz, 0.5 MHz), can be understood with this scheme. Both sets have the same **dq** frequencies according to the observation of just one **dq**−**dq** correlation peak. It is worth noting that in samples labeled in the heme ring only a correlation peak at (5.4 MHz, −1.5 MHz) is assigned to [^{15}N]Hem.

The (2.5 MHz, 0.5 MHz) peak can be associated with the **dq** transition frequency in one spin manifold and the difference of **sq** transition frequencies between [^{14}N]Hem belonging to different sets in the other spin manifold. The possibility that this correlation was an artifact coming from the subtraction background procedure cannot be excluded.

Figure 6 shows a g_Y-HYSCORE spectrum of a ^{14}N naturally abundant model compound sample. The HYSCORE spectra for a magnetic field corresponding to the central feature of the CW spectrum are more complex in all the cases. This is a direct consequence of the multiorientation contribution to the ESEEM signal and prevents us from doing a direct analysis of the observed correlation signals. Nevertheless, g_Y-HYSCORE spectra of selectively ^{15}N labeled samples (see Supporting Information) allow us to assign the appearing correlation signals either to N-Hem or to N-Im nuclei. In particular we want to remark on the [^{14}N]Hem **dq**−**dq** correlation signal. In some spectra of [^{15}N]Im-labeled samples this **dq**−**dq** correlation exhibits a clear doublet structure (two ridges with slightly different slope). As it has been pointed out above, this feature can be interpreted as coming from two nonequivalent pairs of porphyrin nitrogen atoms. Some **sq**−**dq** and **sq**−**sq** ^{14}N correlations can be also identified by taking advantage of the selectively labeled sample spectra. It is worth noting the appearance of two ridges parallel to the negative quadrant diagonal that are separated by twice the Larmor frequency of ^{14}N. These ridges have been identified as [^{14}N]Hem correlations and their lower limit is about (2.3 MHz, −0.4 MHz). Analogous ridges parallel to the diagonal show up in the g_Y-spectra of [^{15}N]Hem-labeled samples. Obviously such ridges are assigned to [^{14}N]Im.

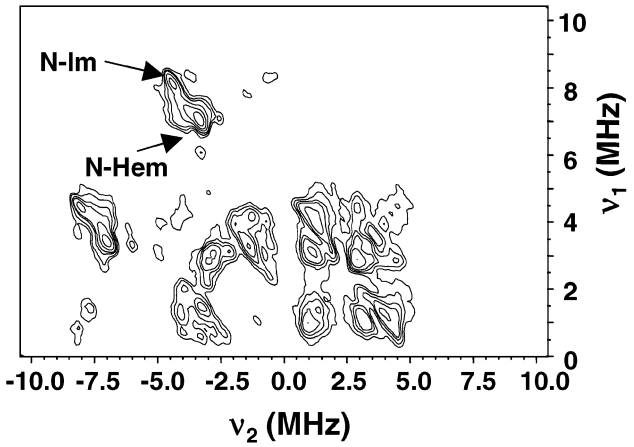

Figure 6. g_Y-HYSCORE spectrum of a ^{14}N naturally abundant model compound sample (for details see Materials and Methods). The static magnetic field was set at 308 mT, and the time separation between the two first pulses was $\tau = 96$ ns. The **dq**−**dq** correlations due to N-Im and N-Hem are indicated.

Cytochrome *b*$_{559}$. The CW-EPR spectrum of Cyt b_{559} in the D1−D2−Cyt b_{559} reaction center sample used for this study is very similar to that of the model compounds. Note that the heme group in Cyt b_{559} is a PPIX (see Figure 1). The principal values of its giromagnetic tensor are $g_Z = 2.98$, $g_Y = 2.25$, and $g_X = 1.53$. This similarity supports the election of our Fe(III)−PPIX-$(Im)_2$ and Fe(III)−CPP$(Im)_2$ complexes as model compounds for Cyt b_{559} and shows that these ferric iron centers have the same electronic state.

As pointed out in the Introduction, some slight differences in the CW-EPR spectrum of D1−D2−Cyt b_{559} reaction center preparations have been detected depending on the final concentration of the β-DM detergent in the sample.[25] Nevertheless no β-DM concentration dependent changes were observed in any of the ESEEM spectra described next.

We have also measured HYSCORE spectra of Cyt b_{559} tuning the magnetic field in the g_X, g_Y, and g_Z resonant positions. In Figure 7 a g_Z-spectrum of Cyt b_{559} is shown. Note the strong similarity with the corresponding spectrum of the ^{14}N naturally abundant model compound (Figure 2). For g_Y- and g_X-HYSCORE spectra such a coincidence also occurs. However, for these two field positions the lines detected for Cyt b_{559} are broader than those for the model compound and then a subsequent loss of resolution occurs.

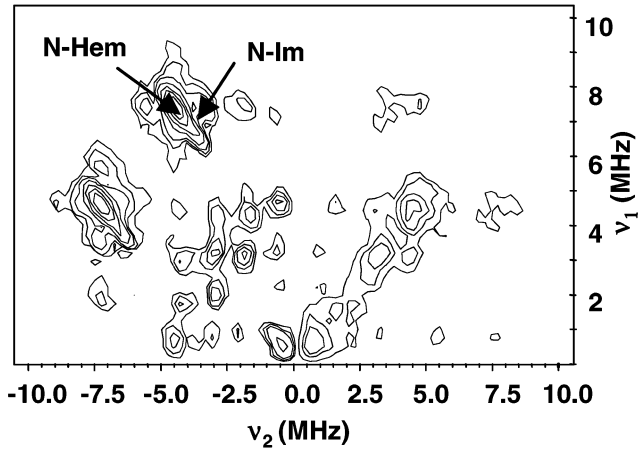

Figure 7. g_Z-HYSCORE spectrum of Cyt b_{556} (for details see Materials and Methods). The static magnetic field was set at 234 mT, and the time separation between the two first pulses was $\tau = 96$ ns. The **dq−dq** correlations due to N-Im and N-Hem are indicated.

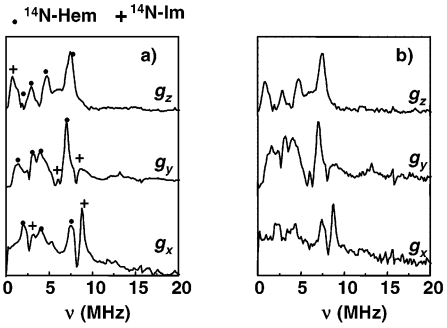

Figure 8. Three pulse 1D-ESEEM spectra of the model compound (a) and Cyt b_{559} (b) for values of the magnetic field corresponding to the principal values of the *g*-tensor. The time intervals between the two first pulses were $\tau = 96$ ns for the g_Z-spectra and $\tau = 208$ ns for the g_X- and g_Y-spectra.

An additional comparison is provided by the 1D-ESEEM spectra, in which the relative intensities of the peaks are more easily quantified. In Figure 8 we present three pulse spectra corresponding to the model compound (a) and Cyt b_{559} (b) with the magnetic field tuned in g_X, g_Y, and g_Z resonant positions. All the observed peaks in the 1D-ESEEM spectra of model compounds have been assigned to N-Im or N-Hem nuclei thanks to the selective ^{15}N labeling performed in the model compound. They can be accounted for by the nuclear frequencies shown in Figures 3 and 5.

As for HYSCORE, 1D-ESEEM spectra of Cyt b_{559} are nearly identical to the ones of the model compound. In Figure 8 the comparison of the 3*p* 1D-ESEEM spectra is given. The lines appear in the same position and display the same relative intensities for all experimental conditions. This also applies to 4*p* 1D-ESEEM spectra (data not shown). Consequently, the assignment of the correlation peaks given in Tables 1 and 2 and the nuclear sublevel schemes shown in Figures 3 and 5 also hold for the Cyt b_{559}.

IV. Analysis of the Spectra

Information about N-Hem and N-Im hyperfine and quadrupolar coupling tensors can be obtained from the analysis of the experimental nuclear frequencies. Details of the procedure we have followed are given as Supporting Information, and only qualitative indications of this analysis and the estimated values of the coupling tensors will be presented in this section. First, we summarize some results given there, which are useful for understanding the procedure.

(i) The direction perpendicular to the porphyrin plane is a principal axis of the *g*-tensor, *Z*-axis. Then, the *X*- and *Y*-principal *g*-tensor axes are in the porphyrin plane. φ_0 denotes the angle between the *X*-principal *g*-tensor axis and the molecular *x*-axis, which coincides with one of the Fe−N-Hem bonding directions. The unpaired electron density is described by $\rho(\vec{r}) = a^2 d_{y'z}^2 + b^2 d_{x'z}^2 + c^2 d_{xy}^2$, where $d_{y'z}$ and $d_{x'z}$ orbitals are obtained, respectively, from d_{yz} and d_{xz} ones by a "counterrotation" of angle $-\varphi_0$ around the *z*-axis. The $a-c$ coefficients can be calculated from the principal *g*-values through the classical Taylor's formulas;[1] in our case the most contributing orbital to the electronic distribution in the ground state is, by far, $d_{y'z}$. Note that the x' and y' axes laying in the porphyrin plane are defined by this counterrotation.

(ii) As a consequence of the symmetry of $\rho(\vec{r})$, the *Z*-axis is also a principal axis of the hyperfine coupling tensor of both, N-Im and N-Hem, types of nuclei. In the *g*-tensor principal axes frame $A_{XZ} = A_{ZX} = A_{YZ} = A_{ZY} = 0$; the hyperfine coupling tensors are determined by A_{XX}, A_{YY}, A_{ZZ}, A_{XY} and $(a^2 - b^2 - c^2)A_{YX} = (a^2 - b^2 + c^2)A_{XY}$.

(iii) The *Z*-direction is also a principal axis of the traceless symmetric quadrupolar coupling tensors of N-Im and N-Hem nuclei. So, in the *g*-tensor principal axes frame $Q_{XZ} = Q_{ZX} = Q_{YZ} = Q_{ZY} = 0$. Alternatively, each quadrupolar tensor can be characterized by its principal values, Q_x, Q_y, and $Q_z \equiv Q_{ZZ}$ ($Q_x + Q_y + Q_z = 0$) and the angle, Θ, that its *x*-principal axis makes with the *g*-tensor *X*-principal axis.

Concerning the axial nitrogen nuclei, it is expected, from previous studies of imidazol-coordinated metals,[35,36] the bonding Fe−N-Im direction is a principal direction and it has the highest principal value (Q_z) in the range between 0.8 and 1.8 MHz. The principal axis with the lowest absolute value (Q_y) is the normal to the imidazol plane, and the third principal axis is the intersection of the imidazol and the porphyrin planes displaying a nearly constant value of $|Q_x| = 0.8$ MHz. These values are compatible with our results.

From the information collected in the literature about the [^{14}N]-Hem nuclei quadrupolar interaction when porphyrin is coordinated with different metals,[6,7,37,38] it can be assumed that the principal direction of the quadrupolar tensor of the [^{14}N]Hem nuclei associated with the principal value with the highest absolute value, Q_x, lies in the porphyrin plane and is perpendicular to the metal−nitrogen bonding direction, being 0.8 MHz $\leq |Q_x| \leq$ 1.1 MHz. The other two principal directions coincide with the normal to the porphyrin plane ($Q_z \equiv Q_{ZZ}$) and with the metal−nitrogen bonding direction (Q_y). Besides, the quadrupolar tensor of both pairs of N-Hem nuclei are related by a $\pi/2$ rotation around the *z*-axis due to the 4-fold symmetry of the porphyrin ring.

N Interaction Parameters in the Model Compound. Information about the hyperfine and quadrupolar tensors of the

(35) Ashby, C. H.; Cheng, C. P.; Brown, T. L. *J. Am. Chem. Soc.* **1978**, *100*, 6057−6063.
(36) Scholes, C. P.; Lapidot, A.; Mascarenhas, R.; Inubushi, T.; Isaacson, R. A.; Feher, G. *J. Am. Chem. Soc.* **1982**, *104*, 2724−2735.
(37) Brown, T. G.; Hoffman, B. M. *Mol. Phys.* **1980**, *39*, 1073−1109.
(38) Van Doorslaer, S.; Schweiger, A. *J. Phys. Chem. B* **2000**, *104*, 2919−2927.

Table 3. Nuclear Spin Hamiltonian Parameters for N-Im and N-Hem[a]

		N-Im	N-Hem	
^{15}N	A_{XX} (MHz)	7.6 ± 0.3	6.8 ± 0.3	
	A_{XY} (MHz)	<1	<2	
	A_{YY} (MHz)	8.7 ± 0.3	6.9 ± 0.5	
	A_{ZZ} (MHz)	7.0 ± 0.3	8.0 ± 0.3	
^{14}N	A_{XX} (MHz)	5.6 ± 0.2	4.7 ± 0.2	
	A_{XY} (MHz)	< 0.7[b]	<1.3[b]	$0.4 < A_{XY} < 1.3$[b]
	A_{YY} (MHz)	6.2 ± 0.3[b]	4.9 ± 0.4[b]	4.9 ± 0.4[b]
	A_{ZZ} (MHz)	5.1 ± 0.5	5.8 ± 0.6	5.8 ± 0.6
	Q_X (MHz)	$\pm 0.8 \pm 0.1$[c]	$0.8 < Q_X < 1.1$[c]	
	Q_{ZZ} (MHz)	$\mp 0.8 \pm 0.1$	-0.4 ± 0.1	-0.4 ± 0.1
	Θ (deg)	65 ± 15	$20-38$	$52-70$

[a] The two columns in [^{14}N]Hem data stand for the two sets of nonequivalent N-Hem nuclei. [b] Scaled from the ^{15}N values. [c] From the bibliography (see text).

interaction nitrogen has been obtained from the experimental results with all these considerations. The values of the coupling tensor components are shown in Table 3. A detailed description of the procedure we have used is given in the Supporting Information; we outline here the main steps.

First, we have analyzed the ^{15}N nuclear transitions. Since in this case $I = 1/2$, the quadrupolar contribution is absent. In principle, the absolute values of $^{15}A_{ZZ}$, $^{15}A_{XX}$, and $^{15}A_{XY}$ for [^{15}N]-Hem and for [^{15}N]Im nuclei can be obtained from the single-crystal-like g_X- and g_Z-spectra. The estimated values for $|^{15}A_{ZZ}|$ and $|^{15}A_{XX}|$ of both types of nuclei are displayed in Table 3 but $|^{15}A_{XY}|$ is determined with a high uncertainty from the g_X spectrum.

To gain information about $^{15}A_{YY}$ and improve the $^{15}A_{XY}$ estimation, we have used the ^{15}N g_Y-HYSCORE signals that are due to molecules with different orientations. g_Y-HYSCORE spectra have been simulated using the formerly estimated $|^{15}A_{ZZ}|$ and $|^{15}A_{XX}|$ values, whereas the values of $^{15}A_{YY}$ and $^{15}A_{XY}$ have been varied in a wide enough interval. By comparison of the simulated spectra with the experimental ones, we have obtained the values for $^{15}A_{YY}$ and $^{15}A_{YX}$ given in Table 3.

It is important to note that all [^{15}N]Hem nuclei are found to be equivalent (see above), and consequently, all of them are described with one set of hyperfine coupling constants. The same applies to both [^{15}N]Im nuclei.

From these values for the hyperfine coupling tensor for ^{15}N an estimation of the hyperfine parameters of ^{14}N nuclei can be done. In this case ($I = 1$) the quadrupolar interaction also has to be taken into account for analyzing the nuclear frequencies.

In first place we have paid attention to the g_Z-HYSCORE spectrum. As we pointed out in Experimental Results, for an orientation of the magnetic field along the Z principal axis of the g-tensor all [^{14}N]Hem nuclei as well as the [^{14}N]Im nuclei are equivalent. Moreover, the values of $|^{14}A_{ZZ}|$, $|Q_z|$, and $|Q_x - Q_y|$ for both, [^{14}N]Hem and [^{14}N]Im, nuclei can be obtained, in principle, from the frequencies of the nuclear transitions displayed in Figure 3. The estimated values of $|^{14}A_{ZZ}|$ and $|Q_z|$ are given in Table 3, but the uncertainty in $|Q_x - Q_y|$ is too high to obtain a significant figure.

Second we have used the information provided by the g_Y-spectra. In particular the presence in the [^{15}N]Im-labeled samples of two different **dq**−**dq** correlation signals associated with [^{14}N]-Hem indicates that the two pairs of [^{14}N]Hem are nonequivalent and that the quadrupolar tensors for these nuclei are strongly anisotropic in the XY plane. This anisotropy is also supported by the **sq**−**sq** ridges in the first quadrant (see Experimental Results), indicating that Q_{ZZ} is not the principal value of the quadrupolar tensor with the highest absolute value (see Supporting Information for details).

Finally, we have analyzed the signals observed in the g_X-HYSCORE spectra. Despite the single-crystal-like nature of these spectra, the symmetry of the interaction tensors provides a complex situation. Since the dominant contribution to the nuclear interaction is the hyperfine one, we have taken advantage of this complexity to obtain information about the orientation of the quadrupolar tensor relative to the g-tensor principal axes (see the Supporting Information for details). As it has been mentioned above, this orientation is given by Θ which is the angle between this x-axis and the g-tensor X principal axis (see Table 3).

In summary, with all these considerations and following the procedure described in the Supporting Information, we have estimated the values of the hyperfine and quadrupolar coupling tensors for N-Im and N-Hem nuclei given in Table 3. Besides, a meaningful interval is obtained for the orientation of the principal axes of the [^{14}N]Hem quadrupolar tensor relative to the g-tensor principal axes.

N Interaction Parameters in Cytochrome b_{559}. As it has already been indicated, the nitrogen nuclear frequencies in Cyt b_{559} are the same as those of the model compound. The same symmetry considerations drawn for the model compound can be used to analyze the Cyt b_{559} spectra. Therefore, the same assignment can be done, and the former analysis is easily extended to this case. It is worth noting the coincidence of the relative intensities of all the peaks in the 1D-ESEEM spectra of both the model compound and Cyt b_{559}. Small changes in the coupling tensors, even if they affect only slightly the nuclear frequencies, have a strong influence on the relative intensities of the 1D-ESEEM signals. Thus, we conclude with a high degree of confidence that the figures displayed in Table 3 also correspond to the nitrogen interaction parameters in Cyt b_{559}.

V. Discussion

On the basis of the information about the coupling tensors with the nitrogen atoms of the porphyrin and imidazol moieties, some structural aspects of our molecules can be discussed.

The orientation of the quadrupolar coupling tensors allows us to determine the orientation of the g-principal axes and the direction perpendicular to the axial imidazol rings. From the quadrupolar coupling with porphyrin nitrogen atoms, the angle between the X principal axis of g-tensor and the bonding directions Fe−N of the porphyrin (that are principal directions of the N-Hem quadrupolar tensor) can be obtained (Θ for N-Hem in Table 3). The orientation of the X principal axis is bound in the region between the dashed lines in Figure 9a (making an angle between 20 and 38° with an Fe−N direction), whereas the solid line indicates its mean orientation. The unpaired electron density is practically in the $y'z$ plane (see Figure 9b) whose orientation can be obtained from the molecular yz plane taking into account the counterrotation (see above).

Attempts have been made to determine the orientation of the magnetic axes in different hemoproteins and model compounds. Using a different methodology, Shokhirev and Walker[39] found an orientation of the magnetic axes in the porphyrin plane similar

(39) Shokhirev N. V.; Walker, F. A. *J. Am. Chem. Soc.* **1998**, *120*, 981−990.

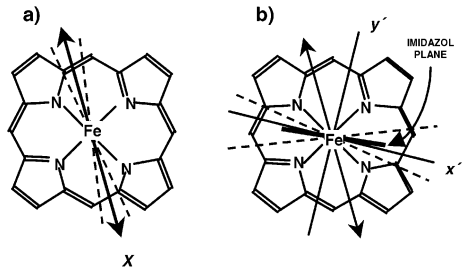

Figure 9. (a) Orientation of the *g*-tensor principal *X*-axis obtained from the N-Hem quadrupolar tensor analysis. Dotted lines indicate a range for the possible orientation of this *X*-axis; the continuous line shows a mean orientation. (b) The thick line indicates the orientation of the imidazol plane (see text). The range of possible orientations is between the dotted lines. The projections of $d_{x'z}$ and $d_{y'z}$ orbitals in the porphyrine plane (labeled as x' and y', respectively), as follows from the analysis of the *g*-tensor, are also indicated.

to that which we obtained. More recently analogous results also have been reported by Astashkin et al.[32] in some model compounds.

The Θ value obtained for N-Im indicates that the angle between the normal to the imidazol plane and the principal *Y*-axis of the *g*-tensor is $65 \pm 15°$ (see Table 3). Taking into account that the two imidazol planes are approximately parallel, as is strongly suggested by the principal *g*-values,[30−32] there are two possible senses of rotation but only in one of them the unpaired electron distribution is in a plane normal to the imidazol ring (see Figure 9b). This arrangement is fully compatible with the hypothesis that the semioccupied orbital orientation is mainly determined by the orientation of the π-orbitals of imidazol whose electrons drive back 3d electrons of Fe^{3+}.[32] In this configuration the imidazol planes approximately bisect the N−Fe^{3+}−N angles. This spatial distribution seems to be stable since it prevents the superposition of the H(C_ϵ) and H(C_δ) charge density of the imidazol moiety with the N-Hem π-orbitals. So, the sense of rotation sketched in Figure 9 looks the most reasonable.

As far as the hyperfine interaction with the nitrogen atoms is concerned, the former results indicate that this interaction is mainly isotropic and the EPR data suggest that the unpaired electronic orbitals have a strong nonbonding character. Any delocalization of the unpaired electron in the adjacent nitrogen *p*-orbitals would produce a noticeable anisotropic contribution to the hyperfine interaction. A rough estimation of the anisotropy of the hyperfine interaction can be done by means of the point−dipole approximation considering that the Fe^{3+} distance to both, N-Hem and N-Im, nuclei is 0.2 nm. In such a case the difference between the highest and lower principal values of the hyperfine tensor would be 2.3 MHz. This is in agreement with the experimental value (see Table 3). All these considerations suggest that the unpaired electron is strongly localized in the iron orbital and that the mixing with the *p*-orbitals of the nitrogen atoms is negligible.

As previously said, the interaction parameters in the case of Cyt b_{559} are the same as those found in the model compound. These results indicate that the structure of the heminic center in the protein should be the same as the one depicted in Figure 9 for the model compound. In the absence of additional steric hindrances, as in the model compound, the axial ligands tend to get an energetically favorable orientation. Nevertheless inside a protein the spatial arrangement of the axial residues can be determined by the protein structure. The structure similarity of the protein and the model compound can be related to the way Cyt b_{559} binds the heme moiety. The Cyt b_{559} consists of two transmembrane-polypeptide subunits (α and β) bounded to the heme center by two histidine residues. This spatial layout lets some degree of rearrangement to α and β subunits. Thus, the orientation of the axial ligands is not significantly hindered by the polypeptide structure and is mainly determined by the porphyrin−imidazol interactions.

Despite the observed principal *g*-value modifications, no differences are found in the interaction parameters when detergent conditions used to stabilize Cyt b_{559} samples are changed. The modification of the g_Z value is about 2%, and the associated change in the ground-state wave function would induce a change of the hyperfine interaction parameters less than 5%, which is lower than the experimental uncertainty (see Table 3).

Finally we will discuss the information derived from the hyperfine nitrogen coupling tensor. As it has been pointed out, the low anisotropic contribution indicates that the unpaired electron is localized in a confined iron orbital with a negligible mixture of nitrogen *p*-orbitals. This makes very unlikely that any substrate or reactive can be located close enough to the orbital occupied by the exchangeable electron for a direct one-step electron exchange. The transfer mechanism could be better understood if it were a multistage complex process where the metal in the heme group of Cyt b_{559} acts only as a final electron reservoir. It has been pointed out in the Introduction that the function of Cyt b_{559} within PSII is not yet well established. The protein can play some structural role, but it seems also possible that the redox capabilities of Cyt b_{559} were exploited in the PSII function. In this sense, it has been suggested that Cyt b_{559} could participate in "secondary" or "alternative" electron-transfer mechanisms when the electron transport from the oxygen-evolving complex is impaired.[15] Such suggestions are in some way supported by our results. The picture of a heme center acting as an electron reservoir with a rather complex electron-transfer pathway is feasible for a process that would only be activated when the main electron transport in PSII is found to be inhibited.

On the other hand, the *g*-tensor principal values obtained from CW-EPR would mainly depend on the metal electronic structure and near environment, whereas measured redox potentials would rather be related with the accessibility of mediators and actual reaction processes in the experiment. Such processes will depend in a complex way on the whole protein conformation. This would explain that although there is some correlation between CW-EPR and redox potential characterizations (both are, in general, affected by conformational and environmental properties), there is not a direct relationship between them. Therefore, it is not possible to label the redox potential form of Cyt b_{559} only from the CW-EPR *g*-values determination, as previously pointed out.[15,18−25] A closer relationship between these two properties should be expected if the reaction mechanism were mainly affected by the heme group redox potential. Indeed, an effort should be made to determine the relevance of the measured redox potentials in the possible functional reactions of this cytochrome.

We also want to point out that our assertion could be considered as a more general conclusion being extended to other

cytochromes. These heme proteins display a wide range of redox potentials, but the principal values of the *g*-tensor of cytochromes are very similar. Despite the lack of information about the hyperfine tensor coupling in different heminic systems, this strongly suggests that the electronic properties of Fe(III) are also very similar in all these systems and no drastic changes are expected in the interaction parameter values. This general phenomenon could be understood if the electron exchanges in cytochromes were complex processes where heme iron acts as a final electron reservoir.

Acknowledgment. The authors are grateful to M. V. Ramiro for skillful technical assistance. We also thank R. Alcalá and J. Ward for their help in the revision of the writing. This work was supported by Dirección General de Investigación (Grant BMC2002-00031) and Gobierno de Aragón (Grant P111/2001), and it has been done within the GC DGA 2002 program of the Gobierno de Aragón.

Supporting Information Available: g_X-, g_Y-, and g_Z-HYSCORE spectra of the ^{14}N natural content and the ^{15}N selectively labeled model compounds and derivation of the nitrogen nuclear transition frequencies and analysis of the spectra. This information is available free of charge via the Internet at http://pubs.acs.org.

JA035364G